

# RSC Advances



This is an *Accepted Manuscript*, which has been through the Royal Society of Chemistry peer review process and has been accepted for publication.

*Accepted Manuscripts* are published online shortly after acceptance, before technical editing, formatting and proof reading. Using this free service, authors can make their results available to the community, in citable form, before we publish the edited article. This *Accepted Manuscript* will be replaced by the edited, formatted and paginated article as soon as this is available.

You can find more information about *Accepted Manuscripts* in the [Information for Authors](#).

Please note that technical editing may introduce minor changes to the text and/or graphics, which may alter content. The journal's standard [Terms & Conditions](#) and the [Ethical guidelines](#) still apply. In no event shall the Royal Society of Chemistry be held responsible for any errors or omissions in this *Accepted Manuscript* or any consequences arising from the use of any information it contains.

# Qualitative Analysis of Some Alkanethiols on Au Nanoparticles during SERS

R.A. Harris\*<sup>1</sup>, M. Mlambo<sup>2</sup>, P. S. Mdluli<sup>3</sup>

\*Corresponding author email: [harrisra@ufs.ac.za](mailto:harrisra@ufs.ac.za); [raharrisphd@gmail.com](mailto:raharrisphd@gmail.com)

<sup>1</sup> University of the Free State, Physics, Nelson Mandela Drive, Bloemfontein, South Africa, 9301

<sup>2</sup> University of Pretoria, Physics, Pretoria, South Africa, 0002

<sup>3</sup> Durban University of Technology, Chemistry, PO Box 1334, Durban, South Africa, 4001

**Abstract-** The surface enhanced Raman spectroscopy enhancement factors (*SERS EF<sub>s</sub>*) for different AuNP-surfactant systems is measured and the observed trend is theoretically and qualitatively investigated. Four thiolated coumarin derivatives (HS-(CH<sub>2</sub>)<sub>11</sub>-NHCO-coumarin, HS-(CH<sub>2</sub>)<sub>11</sub>-NHCO-indole, HS-(CH<sub>2</sub>)<sub>11</sub>-triphenylimidazole and HS-(CH<sub>2</sub>)<sub>11</sub>-hydroquinone respectively) together with a stabilizing surfactant, HS-(CH<sub>2</sub>)<sub>11</sub>-PEG-COOH, were adsorbed in ratios of 1% and 50% onto different sized Au nanoparticles. Similar simulation experiments were done to determine the influence of the nanoparticle-surfactant binding energy (*E<sub>b</sub>*) on *SERS EF<sub>s</sub>*. Other parameters that were qualitatively investigated were the dependency of the Raman enhancement on (a) the size of Au nanoparticles, (b) the relative surface-to-molecule orientation, (c) the molecular orbitals (HOMOs and LUMOs), (d) the molecule electro- and nucleophilic centres and cross-sectional areas as well as (e) the molecular electrostatic potentials. It was observed that each of these parameters contribute to the observed trend and the final Raman signal enhancement.

**Keywords:** SERS, enhancement factor, gold nanoparticles, DFT, Molecular Dynamics, electrostatic potential, HOMO-LUMO, nucleophilic, electrophilic.

## 1. Introduction

Since the discovery of surface-enhanced Raman spectroscopy (SERS) in the 1970's, the use of spectroscopic techniques with intensities augmented by nanostructured metal surfaces have attracted great interest, especially in recent years<sup>1</sup>. By combining electromagnetic radiation with specially prepared nanostructured material's surfaces, the Raman signal can be enhanced by factors<sup>2,3</sup> of 10<sup>4</sup> – 10<sup>6</sup>. Thus, surface molecules that generally have a weak Raman signal at low concentrations or a low Raman scattering cross-section, may be detected.

The enhancement of the Raman signal has led to a highly sensitive and selective surface analysis technique on the molecular level and continues to be a promising technique for future development of analytical applications<sup>4-9</sup>. Since this technique also have many advantages above conventional surface analysis techniques (being non-destructive with a

relatively easy sample preparation process), SERS has already been widely applied in many different fields ranging from sensors for chemical species to new tools for biophysics<sup>10-18</sup>.

Two complementary mechanisms that explain the increase in the Raman signal have been proposed: an electromagnetic interaction model and a chemical interaction model that leads to charge transfer<sup>19, 20</sup>. It has been reported that the electromagnetic interaction of light with surface molecules and atoms may contribute to an increase as high as  $10^6$ – $10^7$  of Raman scattering<sup>21-25</sup>. This occurs as the surface Plasmon gets excited by incident light and amplifies the electromagnetic field of the metal surface. Chemical enhancement contributes up to a factor of  $10^2$  to the increase of Raman scattering, and it happens when the molecule adsorbs strongly on the surface of the metal, leading to changes of its polarizability<sup>26-30</sup>. When the molecule-metal bond becomes too strong, the allowed Plasmon resonance volume is reduced since the vibrating electron's molecular orbitals (MO) decreases in volume. This means that the electrons are held very tightly close to the atomic nuclei that partake in the chemical bond.

The inelastically scattered Raman signal contributes greatly to the increase in the SERS effect and is highly dependent on the nanostructured metal systems present and the particular properties of the particles since it induces greater morphological coupling with the incident radiation. This results in intense spectroscopic signals. The relative molecule-to-surface orientation allows the emergence of new selection rules, resulting in the intensification of the Raman spectrum bands corresponding to the molecular vibrations of the molecular polarizability components perpendicular to the surface<sup>1</sup>.

There has been continued research into the impact of different parameters and properties of the metal nanostructured substrates and their interaction with adsorbed surfactants used in SERS experiments. The surface Plasmon resonance (SPR) in metallic nanoparticles (NPs) is dependent on many factors like the dielectric constants of metals, the crystallographic planes and their orientation, the interparticle distances as well as the size and shape of the NPs<sup>31-33</sup>. The excitation of the SPR results in a strong local electromagnetic field enhancement in the vicinity of the NPs and, more precisely, in the vicinity of the surface metallic atoms. It is this local electromagnetic field enhancement that is responsible for the major enhancement in the Raman spectra of molecules near or attached to the surface of metal nanoparticles<sup>33</sup>. As such, it is expected that any modification of the localized electrostatic potential and

electromagnetic field due to surface adsorbed molecules, will directly influence the SPR and consequently the Raman signal enhancement.

The objective of this study is to investigate the effect that the individual molecular structures has on SERS. Therefore very similar molecules (except for a slight change in the tail-end) was chosen. In the context of the two proposed SERS mechanisms it is important to investigate how the ligands interact with the AuNP surface as the binding modes change with an increase in the number of bound ligands on the NP surface. By changing the number of ligands on a given Au NP surface area, the binding modes (orientations) and consequent binding energies (BE) per ligand are expected to change. Consequently the chemical interaction and charge-transfer will also be altered. Therefore, in this study the influence of ligand concentration on AuNPs is investigated in the broader context of studying the ligand properties in relation to the observed SERS. As such the ligand concentration is varied and not the Au NP concentration as is usually done. Also alkanethiols have an ability to form self-assembled monolayers (SAMs) on the surface of nanoparticles, using the thiol head group which results in specific orientations or projections of an alkanethiol. The orientation is governed by a number of factors: (1) the energetically favoured lattice plane for adsorption of a thiol-head group (dictated by the NP shape and size); (2) surface coverage of the whole NP and (3) the presence of the other functional groups on the alkanethiols which may interact with the NP surface. The resulting SAMs provide an easier method to quantify their contribution to SERS due to the manner in which they adsorb on the surface of the NP, yielding a uniform contribution towards the EF. Alkanethiols also guide the growth, increase the stability and also provide additional stability to nanosystems

Therefore, this investigation reports on the influence that four similar surfactants with slight modifications in the tail-end have on the enhancement factor in SERS. These molecules are adsorbed onto AuNPs. It is expected that these modifications will alter the electronic properties of the system during the Au-S bond formation. The properties that are investigated are the surfactant-AuNP BE per ligand, relative surface-to-molecule orientation (as a function of AuNP size), the molecular orbitals (HOMOs and LUMOs), the molecule electro- and nucleophilic centres and cross-sectional areas as well as the molecular electrostatic potentials. The molecules selected for this study are HS-(CH<sub>2</sub>)<sub>11</sub>-NHCO-coumarin, HS-(CH<sub>2</sub>)<sub>11</sub>-NHCO-indole, HS-(CH<sub>2</sub>)<sub>11</sub>-triphenylimidazole and HS-(CH<sub>2</sub>)<sub>11</sub>-hydroquinone.

## 2. Experimental and Computational Methods

### *Experimental Methods*

After AuNPs were synthesized, 8 different surface conjugated AuNP systems were prepared. The 8 systems consisted of AuNPs that were functionalized with 4 different thiolated coumarin derivatives at 2 different ratios of PEG to thiolated coumarin derivatives. The ratios that were used were 1% and 50% respectively and the different thiolated coumarin derivatives were HS-(CH<sub>2</sub>)<sub>11</sub>-NHCO-coumarin, HS-(CH<sub>2</sub>)<sub>11</sub>-NHCO-indole, HS-(CH<sub>2</sub>)<sub>11</sub>-triphenylimidazole and HS-(CH<sub>2</sub>)<sub>11</sub>-hydroquinone. SERS was done by obtaining Raman spectra *via* a 400 benchtop Perkin Elmer Raman Station spectrometer. The Raman spectra was used to calculate the enhancement factors (EF). AuNP absorption spectra were also obtained to investigate electron sharing between the AuNP and adsorbed ligands. All the details for sample preparation, functionalization, characterization and calculations can be seen in the supporting information.

### *Computational Methods*

In order to qualitatively study the EF dependency on the size of AuNPs, the relative surface-to-molecule orientation, the adsorption BE per ligand, the MOs, the molecule electro- and nucleophilic centres as well as the molecular electrostatic potentials, different sized AuNPs, were modelled. Truncated octahedral AuNPs of different sizes with diameters of 2.80 nm, 5.25 nm, 7.10 nm and 9.6 nm (cluster sizes ranging from Au<sub>459</sub> up to Au<sub>33469</sub>) were constructed (figure 1) and surfactant adsorption was simulated (*via* a simulated annealing Monte Carlo scheme) and surfactants were allowed to be adsorbed in different ratios of PEG-molecules to surfactant-molecules onto the AuNP surfaces (see supporting information for computational details). The following PEG to surfactant molecule ratios were used: 100%, 90%, 74%, 50%, 24%, 2% and 0%.

Since a trade-off exists between simulation accuracy and computational time it becomes increasingly more difficult to accurately execute molecular mechanics and dynamics calculations on large atomic systems. Therefore the aforementioned NP sizes were selected

and simulated. It was found that for the largest of the four the computational time (wall-clock time) became too large to continue with even larger sizes. However, although these simulated NP sizes are not exactly the same as the experimental investigation, the same trends (small nanoparticles vs large nanoparticles) can still be observed as discussed below.

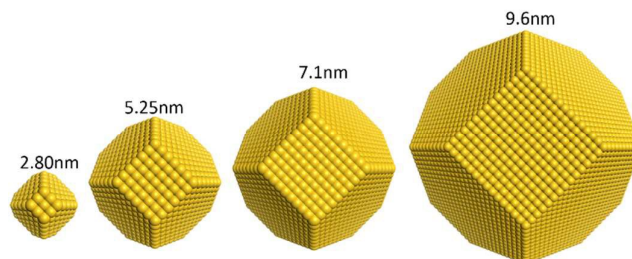


**Figure 1:** Truncated octahedral Au nanocrystals of different sizes (from left, diameter = 2.80 nm, 5.25 nm, 7.10 nm and 9.60 nm).

*Molecular mechanics* were used to determine the optimum geometries for each of the resulting PEG, surfactant-NP systems and *molecular dynamics* simulations were performed on each of the systems to arrive at the final, energy-optimized configurations. The BEs between the surfactants ( $E_s$ ) (PEG and all four alkanethiols) and the NP surface ( $E_{np}$ ) were then calculated per ligand. To investigate the molecular structure, MO, electron density, electrostatic potential as well as the electro- and nucleophilic centres of each molecule, calculations were done within the framework of the *density functional theory* (The computational details are available in the supporting information).

### 3. Results and discussion

The synthesis and experimental results (including AuNP characterization) of the different AuNP sizes are reported in the supporting information where table S1 shows the optical properties of all synthesised AuNP conjugate systems. The prominent surface Plasmon peak ranging between 520 to 537 nm was observed for all NP conjugate systems. Theoretical Raman spectra for each of the thiolated coumarin derivatives are shown in figure S2. The spectra in figure S2 were significantly applied to assign experimental Raman peaks resulting from each surfactant. The experimental Raman spectra (figure S4, S6, S8 and S10) were used to calculate the EF values from the intensities of  $\nu(\text{C-H})$  for 1% and 50% of HS-(CH<sub>2</sub>)<sub>11</sub>-NHCO-coumarin, HS-(CH<sub>2</sub>)<sub>11</sub>-NHCO-indole, HS-(CH<sub>2</sub>)<sub>11</sub>- triphenylimidazole and HS-(CH<sub>2</sub>)<sub>11</sub>-hydroquinone respectively (from hereon only referred to as coumarin, indole,

triphenylimidazole and hydroquinone). These molecules were adsorbed onto AuNPs with average sizes of 14.8, 28.5 and 40.2 nm respectively. (The co-stabilizing surfactant was HS-(CH<sub>2</sub>)<sub>11</sub>-PEG-COOH, from hereon only referred to as PEG). Figure 2 shows the resulting EFs by altering surfactants, AuNPs sizes and ratios PEG to coumarin, triphenylimidazole, indole and hydroquinone.

An increase in EF is observed for all AuNPs (14.8, 28.5, 40.2 nm) as the percentage of coumarin was increased from 1% to 50 %. The most significant SERS effect is observed for AuNPs with an average size of 14.78 nm. The EF is found to decrease as the size of the AuNPs increase from an average size of 14.78 nm to 40.16 nm. This is attributed to the fact that, even though larger NPs should lead to an increase in the local electromagnetic field enhancement, the convex shape of the surface also becomes much flatter for larger NPs. Thus the NPs will absorb less light which leads to much less inelastic scattering of light on the surface<sup>33-37</sup>. This weakens the electromagnetic field on the surface and reduce the overall SERS intensity. A contrary argument can be made that the enhancement at the sharp edges should increase as the NP becomes more "planar" (with an increase in size) and that, since SERS predominantly probes the "hottest" sites on the NP, it is expected that the enhancement should also increase. However if the amount of absorbed light (overall) is decreased the resulting inelastic scattering should also decrease and consequently such a SERS enhancement will not occur.

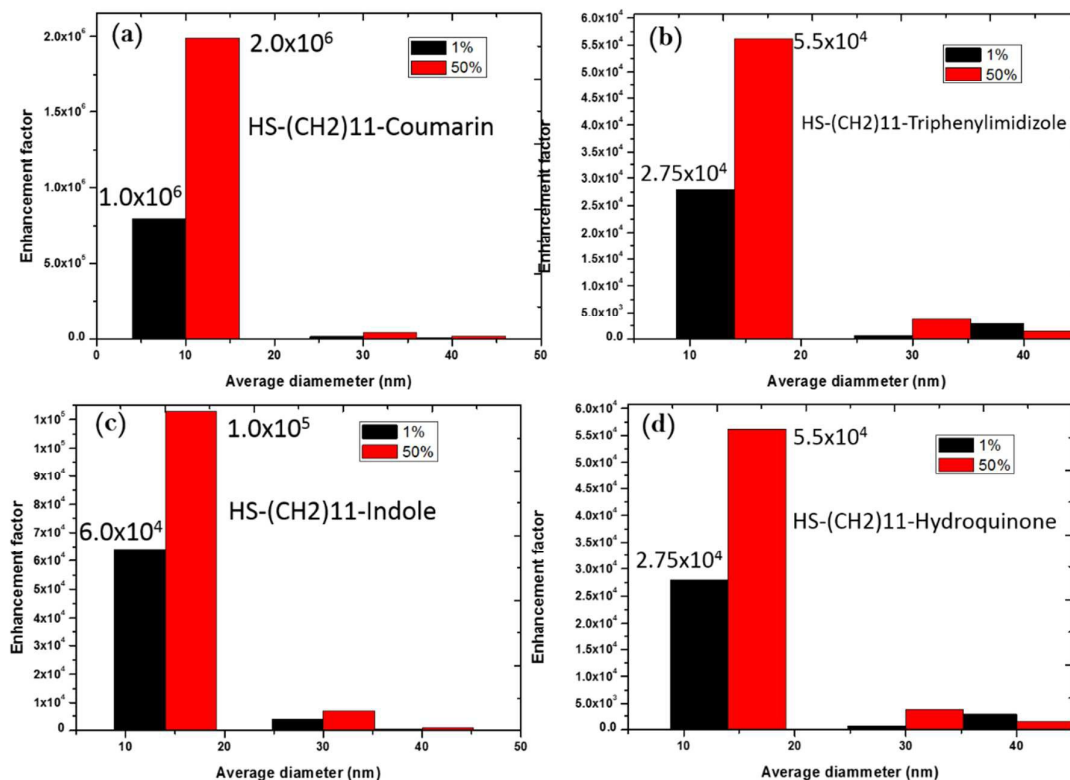


**Figure 2:** Enhancement factors for coumarin, indole, triphenylimidazole and hydroquinone by changing: (1) the surface-adsorbed molecule percentage from 1% to 50% and (2) by changing the AuNP size.

It is expected that, as the NP becomes larger and more planar, the sharp edges/points will be spread out across a larger volume. Therefore localized electromagnetic fields that may have overlapped at the sharp points and led to localized field enhancement for small NPs will no longer overlap for larger NPs and consequently a reduction in the overall SERS is expected.

From figure 2 the thiolated coumarin molecules may be ranked from the molecule that produces the highest EF to the lowest EF as follows: coumarin, indole, triphenylimidazole and hydroquinone roughly the same.

Figure 3 shows the calculated BE per ligand for the smallest of the simulated AuNPs (2.8nm, Au<sub>459</sub>). Similar to the “real-world” experiment, in the simulation experiment the ratio of PEG/surfactant was also allowed to vary between 0% (i.e. 100% PEG) and 100% (i.e. 0% PEG) but with much smaller increments.

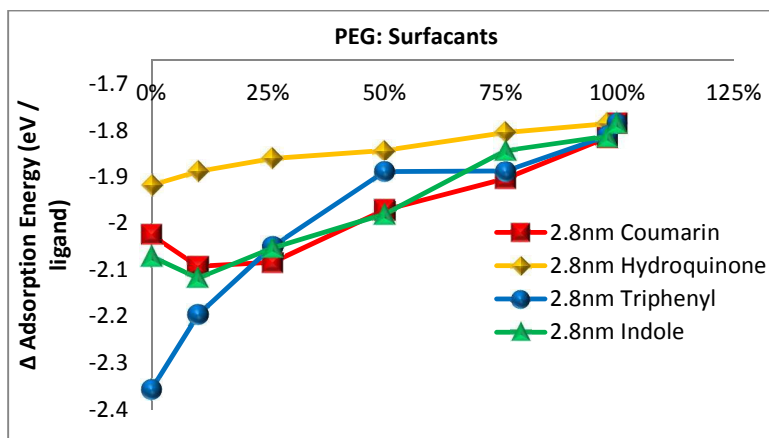


**Figure 3:** Calculated binding (adsorption) energies per ligand for the smallest of the simulated nanoparticles, i.e. 2.8 nm, Au<sub>459</sub>.

It is seen that at a molecular concentration of 50%, both indole and coumarin have the largest and roughly the same adsorption energies (BEs) (-1.98 eV/ligand). This is followed by triphenylimidazole and then hydroquinone with BEs per ligand of -1.89 and -1.84 eV/ligand respectively. These values are well in line with reported values for the Au-S bond calculated on very small Au (38-55 atoms) and Ag (13 - 309 atoms) clusters by Becerril *et al.* [38] and Barnard *et al.* [39]. A weaker interaction between the sulphur atom (S) and the metal surface leads to a lesser sharing of the available electrons in the Au-S bond that partakes in the SPR. Thus the ligand-AuNP bonding orbitals will be slightly shifted towards the S atom in this bond.

Consequently the localized polarizability will be weakened which, in turn, will also weaken the SPR. It is therefore expected that, in this case, the Raman enhancement will be weaker for molecules with a lower BE per ligand. As was reported in Figure 3, this is the case with both, triphenylimidazole and hydroquinone having the weakest EF of only about  $5.5 \times 10^4$  at a 50% molecular concentration and  $2.75 \times 10^4$  at a 1% molecular concentration. Contrary to this, both coumarin and indole show high EF values of  $2.0 \times 10^6$  and  $1.0 \times 10^6$  respectively for 50% molecular concentrations and  $1 \times 10^6$  and  $6.0 \times 10^4$  for a 1% molecular concentration, which agrees with the higher BE values for these two molecules in figure 3.

Figure 3 was expanded around the 1% area, and is shown in figure 4. The experimental trend of the EF persists with the BE values at 2% molecular concentration with coumarin having

the highest BE, -1.815 eV/ligand (and highest EF), followed by indole, -1.813 eV/ligand, then triphenylimidazole, -1.811 eV/ligand, and then hydroquinone, -1.785 eV/ligand.

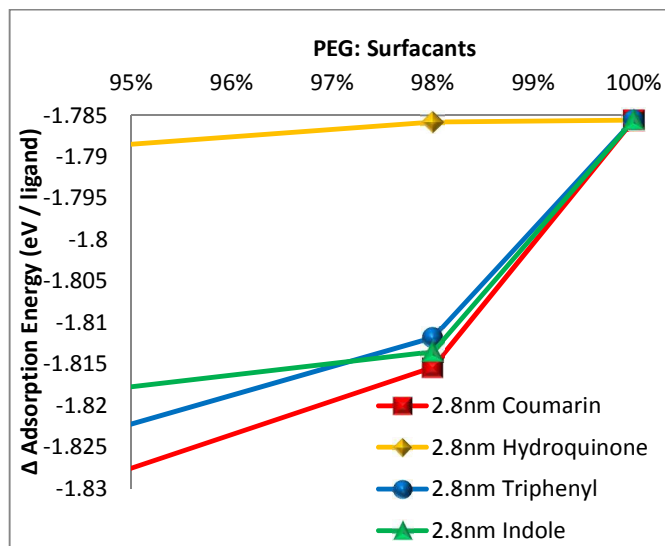


**Figure 4:** Calculated binding (adsorption) energies per ligand for the smallest of the simulated nanoparticles, i.e. 2.8 nm, Au<sub>459</sub> around 2 % molecular concentration (i.e. 98% PEG and 2% surfactant).

When the bond strength is too large, as is the case for large NPs, it hinders the collective resonance of the electrons at the surface of the metal particles. This will detract from the enhancement. Figure 5 shows the calculated BEs/ligand for the system where the AuNP size was roughly doubled (from 2.8 nm to 5.25 nm). It can be seen that the BE per ligand have increased from the reported values by Becerill *et al.*<sup>38</sup> and Barnard *et al.*<sup>39</sup> for the Au-S bond. Most of the ligands now lay flat on the surfaces of the NPs for larger NPs (figure 10). Thus, not only do less surfactants bind per NP but also other bonds may form between the NP surface's Au atoms and the ligand's CH groups, N and O atoms.

Here, triphenylimidazole has the largest BE value at 50% of -2.92 eV/ligand roughly twice the value reported for the smaller AuNP. This is followed by hydroquinone at -2.56 eV/ligand, then indole at -2.45 eV/ligand and coumarin at -2.27 eV/ligand. The BEs per ligand follow the same trend as the experimentally measured EFs, but in reverse order: coumarin has the lowest BE per ligand (with the largest EF), followed by indole, hydroquinone and triphenylimidazole.

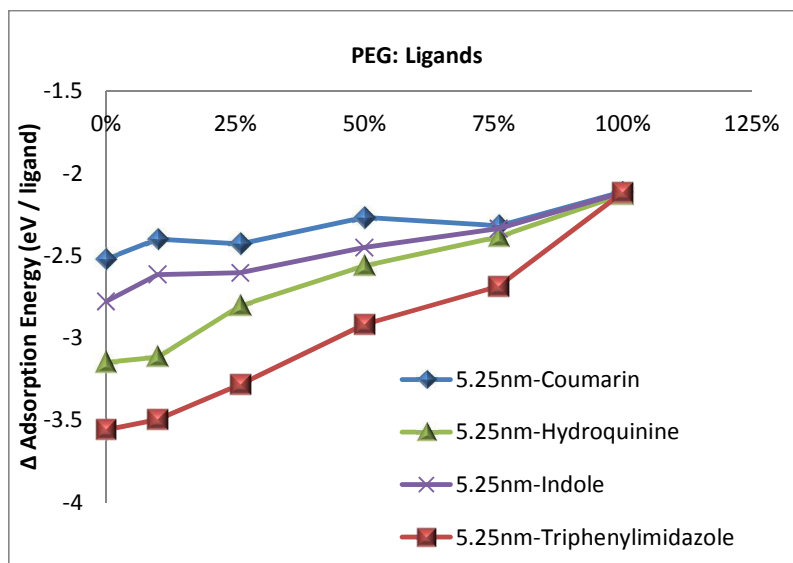


**Figure 5:** Calculated binding (adsorption) energies per ligand for larger Au nanoparticles of 5.25 nm in diameter.

Thus when the Au-S bond strength becomes too large, the collective resonance of the free electrons at the surface of the metal NPs is reduced. It can therefore be hypothesized that the BE per ligand should not be too small nor too large in order to observe meaningful enhancement.

A large spread in the resulting BE per ligand is observed (for both small and large NP systems). For any given size of a NP, (where  $d$  = NP diameter) a fixed number of adsorbed surfactants exists before saturation occurs, i.e. before the NP is electro-chemically stabilized. For any given size of NP, the available surface area for ligand adsorption is fixed. Thus the number of allowed adsorption sites are also fixed and consequently any given size of NP can only adsorb at maximum a fixed number of surfactants,  $N_s$  (= maximum allowed adsorbed surfactants). It is therefore clear that the real number of adsorbed surfactants ( $N$ ) should have an upper limit where

$$N \leq N_s = f(d) \quad (1)$$

This mathematical limit also represents the point of maximum stability for the NP, where the total surface area is effectively electro-chemically passivized. Thus, an upper limit could be set on the BE per ligand ( $E_{b \max}$ ) where, for a given  $d$ , the maximum allowed number of surfactants  $N_s$  have been adsorbed:

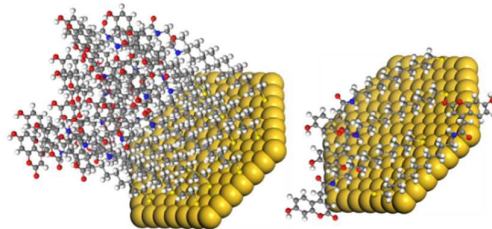
$$E_{b \max} = \frac{E_{b \text{ total}}}{N_s} \quad (2)$$

However, the *real* number of adsorbed ligands,  $N$ , will almost always be less than the ideal saturation adsorption ( $N_s$ ) and is also a function of various other variable parameters including ligand concentration,  $L_c$ , as well as binding geometry,  $G$ . For example, much more ligands can be adsorbed onto surface perpendicularly rather than planar, figure 6. Therefore the binding geometry directly affects the real number of adsorbed ligands. Since the real BE per ligand ( $E_{b \text{ real}}$ ) is a function of the real number of adsorbed ligands (which, in turn, are associated with variables  $G$  and  $L_c$ ) this should vary as the binding geometry changes with an increase in size as well as with a change in the ligand concentration:

$$E_{b \text{ real}} = \frac{E_{b \text{ total}}}{N} \quad (3)$$

Thus it is expected that the BE per ligand should have a relatively large spread as both the concentration of adsorbed surfactants as well as the binding orientation changes when the NP size increases. Therefore; the BE per ligand are dependent on both the total number of ligands bound to the NP surface as well as the type of ligand-atom binding (Au-S, Au-O, Au-CH or Au-N).

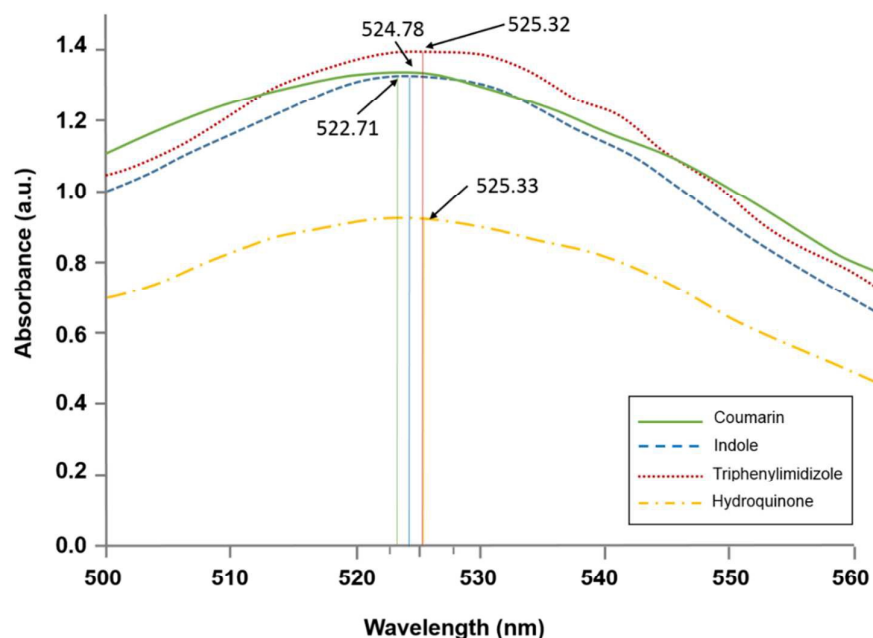
It is expected that the correlation between the bonding strength and the EFs through electron sharing should also track the changes in the absorption spectrum for the different ligands. Figure S11 to S14 in the *supporting information* show the absorption spectra for the different ligands, ligand concentrations and NP sizes.



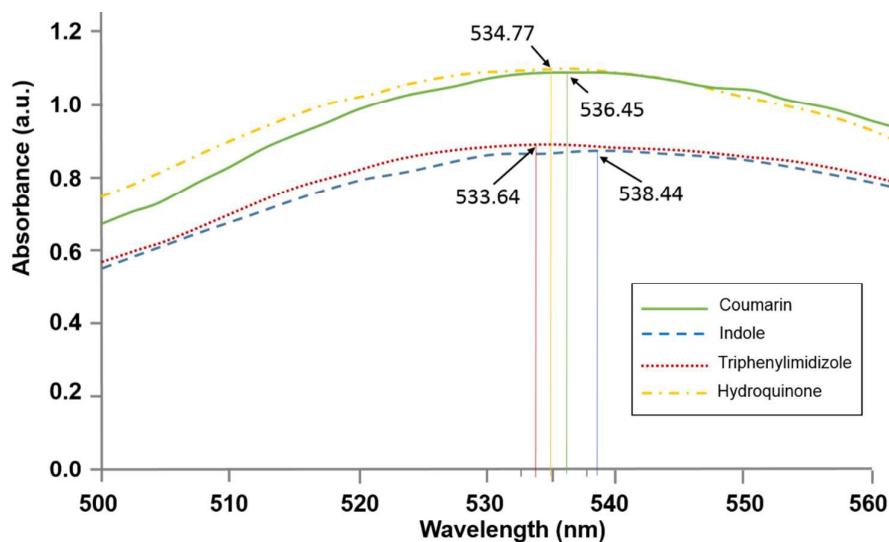
**Figure 6:** Much more ligands can be adsorbed onto a given surface if they are adsorbed perpendicular (left) rather than planar (right).

Figure 7 and 8 are presented as summaries of these spectra for all 4 ligands at a 50 % concentration and a NP size of 14 nm (small) and 40 nm (large) respectively. By considering the wavelengths of maximum absorption, a similar trend is observed as in the BE diagrams. For smaller NPs, coumarin absorbs the highest energy photons (at 2.38 eV, 522 nm) then indole (2.366 eV, 524 nm) followed by triphenylimidazole (2.360 eV, 525.32 nm) and hydroquinone (2.360 eV, 525.33 nm) respectively. It is observed that triphenylimidazole and hydroquinone have roughly the same BEs/ligand and therefore require the same energy photons.

For larger NPs (figure 8; 40 nm), similar to the BE diagram, triphenylimidazole absorbs the highest energy photons (2.323 eV, 533.64 nm), then hydroquinone (2.318 eV, 534.77 nm). There is a slight change in the order of coumarin and indole though. In the absorption spectra coumarin absorbs the higher energy photons (2.313 eV, 536 nm) and then indole (2.304 eV, 538 nm). These differences are attributed to the subtle differences in both the lowest unoccupied MOs (LUMOs) as well as the electrostatic potentials of these molecules which will be discussed later. The maximum absorption wavelength has shifted from 520 - 530 nm (for small NPs) to 530 - 540 nm for larger NPs.



**Figure 7:** Absorption spectrum at the peak absorption wavelength for 50 % coumarin, indole, triphenylimidazole and hydroquinone respectively for 14 nm (smaller) AuNPs.



**Figure 8:** Absorption spectrum at the peak absorption wavelength for 50 % coumarin, indole, triphenylimidazole and hydroquinone respectively for 40 nm (larger) AuNPs.

The red-shift in AuNP absorption wavelength towards lower energy photons and the relation between the BE and the EFs through electron sharing, are explained as follows:

When the BE per ligand is small (as is the case in small NPs) the shared electron is located much closer to the ligand atom (for example the S atom – figure 9 (a)). Thus the bonding-orbital (BO) is closer to the ligand in energy space, figure 9 (c). During AuNP photon absorption, a high energy photon (short  $\lambda$ ) is required to draw and deposit the shared electron away from the ligand and closer to the metallic surface into the sea of delocalized electrons. For bulk Au, it is well known that the multitude of allowed quantum energy states overlap to form an energy band (conduction band - CB) wherein the delocalized electrons may exist that overlaps with the localized electron energy band (valence band – VB). This is also true for large NPs. However, as the size of the NP decreases and the number of atoms and delocalized electrons decreases, the size and position in energy space of this band also changes. In figure 9 (c) this is exaggerated and only a few allowed quantum energy levels are shown. Electrons relatively far away from the Au-ionic cores in energy space may then (in conjunction with other delocalized electrons) readily partake in SPR. The degree to which it will partake in SPR is directly dependant on the bond strength between the delocalized electron and the surface Au ions. Thus for smaller BE's per ligand the electron will readily partake in SPR.

Contrary, for larger NPs the value of the BE per ligand is much larger since most of the ligands lay flat on the NP surface and less ligands are bound to the surface. Therefore other atoms (other than S) may also interact with Au atoms. Thus the shared electron's BO is located much closer to the Au atom, figure 9 (b), and the BO has also shifted closer to the metallic delocalized electronic orbitals, figure 9 (d), in energy space.

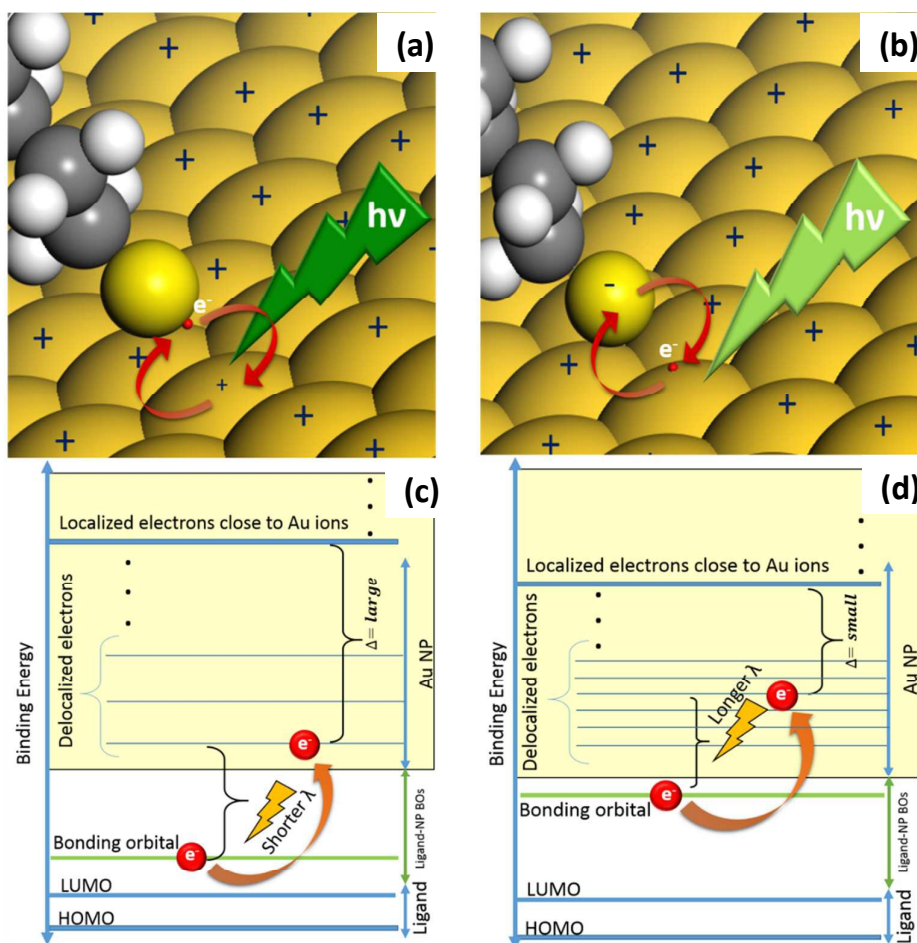


**Figure 9:** For smaller BE/ligand the shared electron is closer to the bonding atom in real space (a) and the bonding orbital closer to the ligand molecular-orbitals (c) in energy space. A higher energy photon is absorbed to excite electron into metallic CB. For a larger BE/ligand the shared electron is closer to the metallic atom in real space (b) and the bonding orbital closer to the metallic delocalized CB in energy space (d); requiring a lower energy photon during excitation into the CB.

Thus, a lower energy photon is required to excite the electron from the BO into the metallic conductor CB. However, since the average electrostatic potential is also larger around any

particular atom the shared electron is now also bound much closer to the Au ionic-core and it will therefore not readily partake in any SPR.

Figure 10 shows the resultant energy- and geometry- optimized AuNP systems for the small and large NP diameters after coumarin has been adsorbed onto the surface in a molecular concentration of 50%. The surface-to-molecule orientation on the smaller NP is more perpendicular to the metal surface compared to the planar/flat orientation of the large AuNP system. The molecule-to-surface orientation allows the emergence of new selection rules and consequently the intensification of the Raman spectrum bands corresponding to the molecular vibrations of the molecular polarizability components perpendicular to the surface<sup>1</sup>. For this reason, more peaks are observed in the Raman spectra (supporting information, figure S4, S6, S8 and S10) for larger NPs in the band from 500 to 1700  $\text{cm}^{-1}$ . However, the convex shape of the surface also becomes much flatter for larger NPs. Thus the NPs will absorb less light which leads to much less inelastic scattering of light on the surface.<sup>33-37</sup>

It is therefore expected that for these molecules the smaller AuNP systems will have a much larger EF compared to the large diameter NPs. The same molecule-to-surface orientation was observed for all the other molecules under investigation and figure S15 to S18 in the *supporting information* summarizes these optimized geometries for each investigated surfactant respectively.

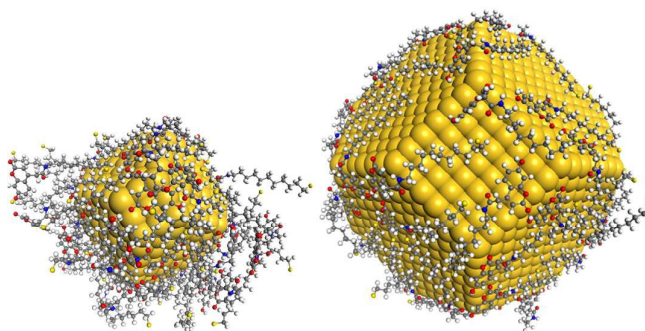


**Figure 10:** Relative molecule-to-surface orientation for different sized AuNPs. (*Left*) the smaller nanoparticle shows a perpendicular molecule-to-surface orientation and (*Right*) the larger nanoparticle shows a planar/flat molecule-to-surface orientation.

To investigate the role that the MOs may play in SERS, the highest occupied MOs (HOMOs) and the lowest unoccupied MOs (LUMOs) for each surfactant were calculated *via* DFT and are presented in figure 11. All the HOMOs are centred on the S atoms. The LUMOs are

centred on the carbon rings at the surfactant tail. This indicates that electrons from the S atoms will have to migrate towards the carbon ring structure to fill the unoccupied orbitals once they have been excited. When the surfactant binds to the AuNP through the S atom in a perpendicular fashion (as is the case for smaller NPs) the shared electrons are closer to the Au atom in both physical and energy space. These electrons may then either move away from the metallic surface upwards towards the LUMO or downwards towards the metallic surface into the CB. It will be more energy efficient (for smaller NPs) that the shared electron will simply be excited directly into the metallic CB.

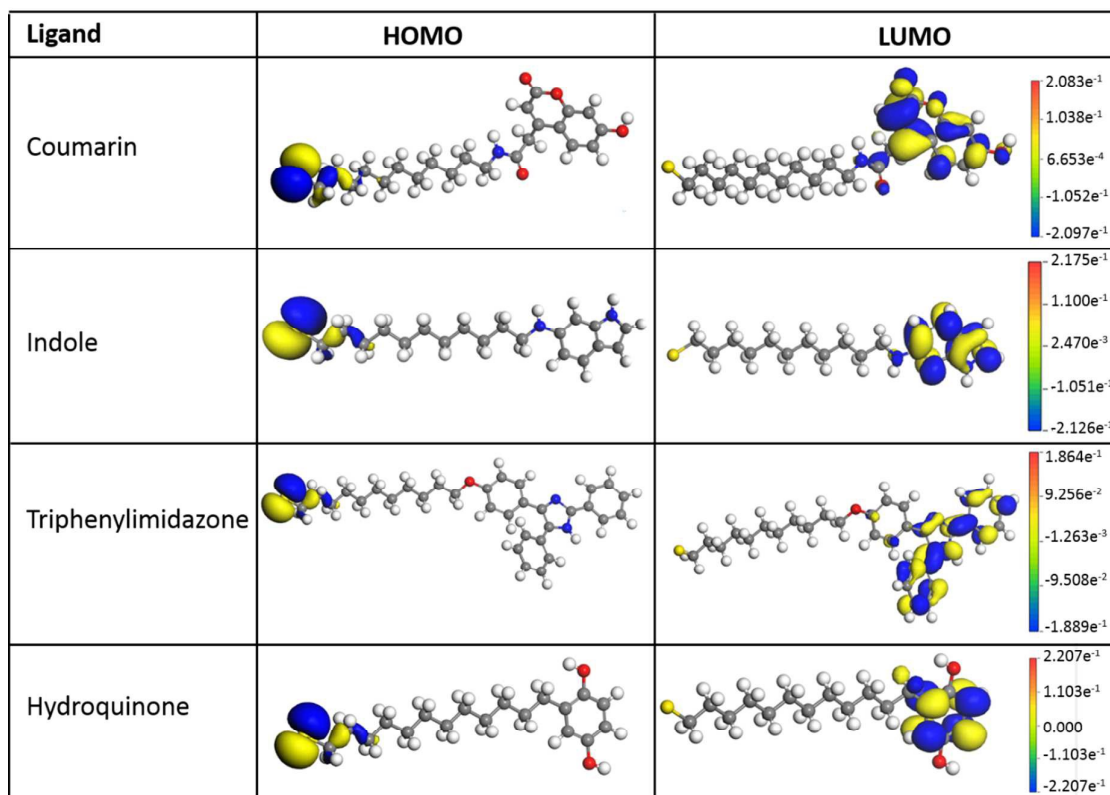


**Figure 11:** (Left) Highest occupied molecular orbitals (HOMO) and (Right) lowest unoccupied molecular orbitals (LUMO).

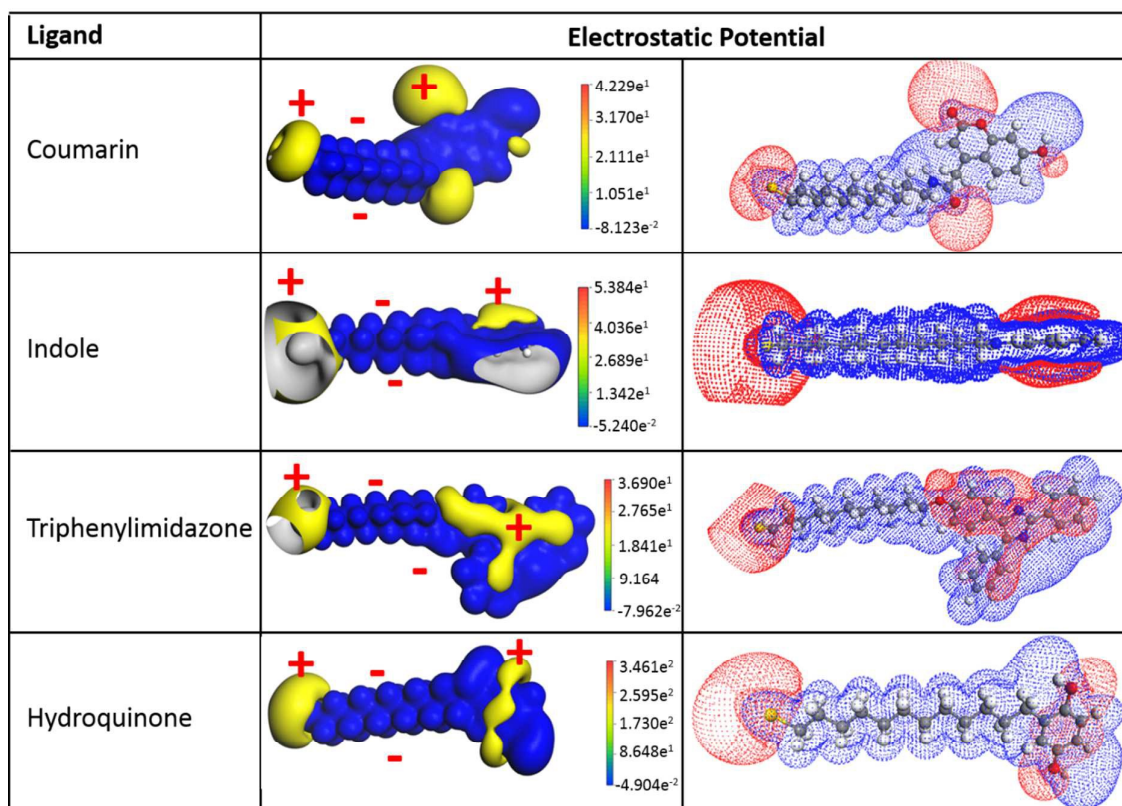
However, when the surfactant lays flat on the surface of the NP (as is the case for larger NPs) the distance (in physical and energy space) between the LUMO and the metallic CB become comparable. As such an excited electron has an equal probability to either migrate towards the LUMO or to be excited into the metallic CB. Consequently the number of electrons that are added to the metallic CB that will partake in SPR has reduced in comparison to smaller NPs.

The electrostatic potential (EP) is another factor that plays a role in surfactant-AuNP interaction. The distribution of electric charge around a molecule creates an EP in the surrounding space. A positive EP will repel other positive charges in that region of space and a negative EP will attract other positive charge. Similarly the positive vector component of incident electromagnetic radiation will repel positive charge and the negative vector component of incident electromagnetic radiation will attract positive charge.

Figure 12 shows the DFT calculated isosurfaces of the EP for the 4 molecules under consideration. On the left side a solid isosurface is presented and on the right side a dotted isosurface so that the individual atomic positions may be seen in relation to the EP surface. The yellow and red shades represent a positive EP and the blue shade represents a negative EP. For all 4 ligands, a positive EP exists around the S atoms. However, this potential-surface does not form a solid sphere around the S atom for any of the 4 molecules. The unique shapes of each of these potential surfaces show areas with zero EP and is directly responsible for the orientation (directionality) and bond strength between the Au-S atoms. This zero EP is smallest for coumarin.

At the tail-end of the ligands, another positive EP surface exists close to the carbon-rings. However there is a crucial difference between these positive EP surfaces: for coumarin and indole these surfaces are stacked in a polar configuration. This means that the EP has a configuration where there exists two outer surfaces of positive potential and one inner surface with a negative potential. Contrary to this, for hydroquinone and triphenylimidazole a positive EP *surrounds* the negative potential surface (like a doughnut shape). This polar configuration for coumarin and indole contributes to the relatively larger EF that was observed for these 2 molecules compared to hydroquinone and triphenylimidazole. The stacked polar configuration leads to an enhancement of the localized EP compared to the doughnut shaped configuration where the positive potential is “*smearred out*” across the entire molecule tail.

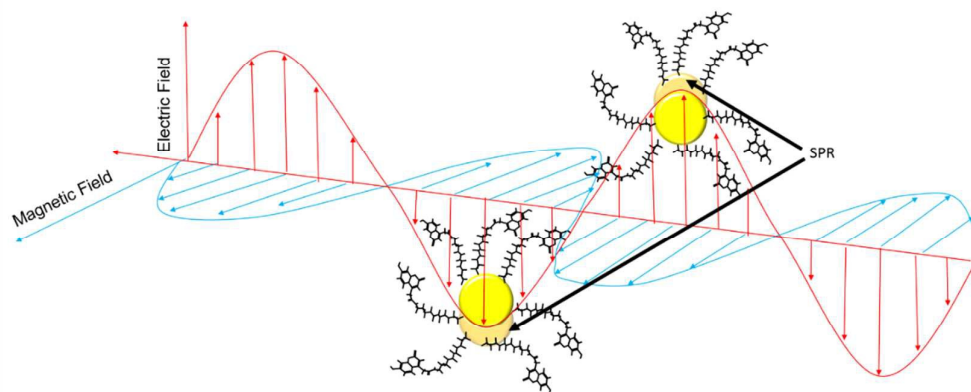
Since the total positive electrostatic surface area of coumarin is larger than that of indole, coumarin has a factor of  $2 \times 10^6$  enhancement compared to the  $1 \times 10^5$  enhancement for indole. The larger cross sectional area allows for an extended interaction with electromagnetic radiation.



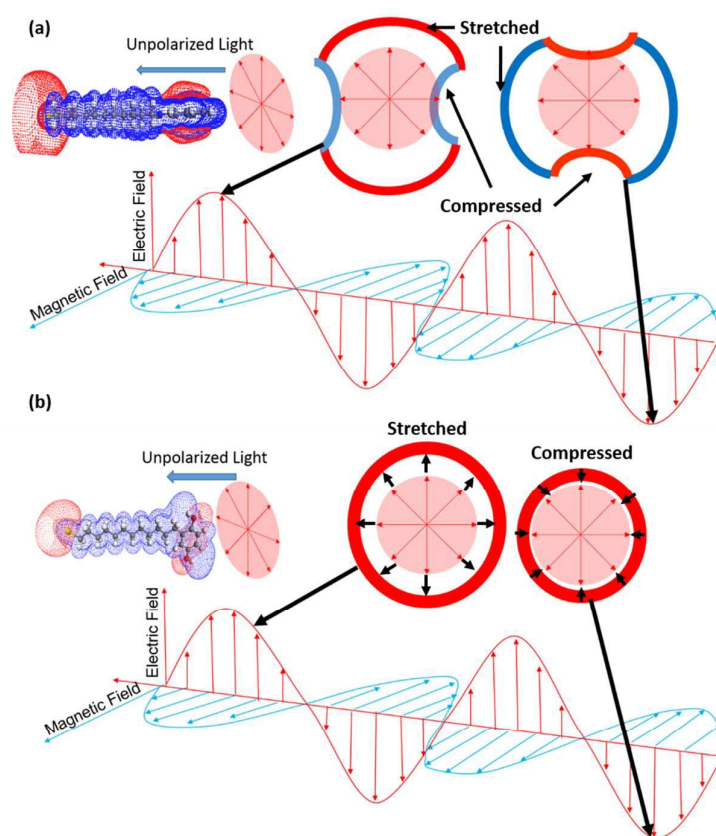
**Figure 12:** Electrostatic potential. The yellow and red shaded areas indicate a relative positive electrostatic potential and the blue areas are negative electrostatic potentials.

Figure 13 shows the expected SPR when the electric field component of radiation interacts with the AuNP. As this component cycles from positive through zero to negative values and back, all molecules attached to the surface will vibrate accordingly. However the electromagnetic radiation will also interact with the molecules themselves, changing the energetics of the MOs.

Figure 14 (a) shows when unpolarised radiation interacts with the polar-stacked tail end of the indole molecule: the tail will be stretched and compressed as shown. Contrary, unpolarised radiation interacting with the doughnut EP on the hydroquinone molecule's tail will expand and compress the tail symmetrically in all directions, figure 14 (b).



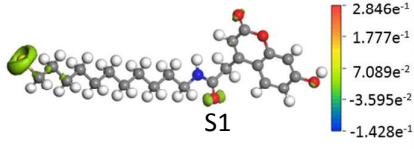
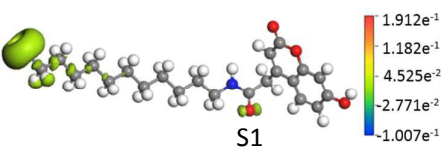
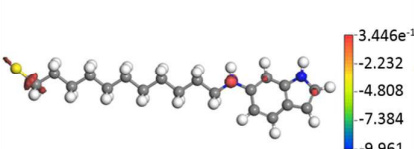
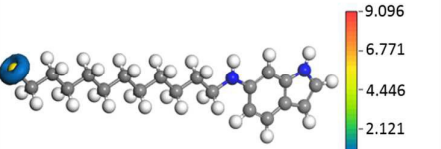
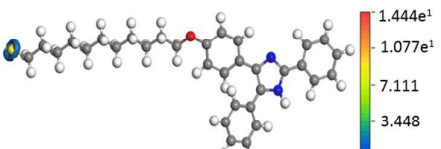
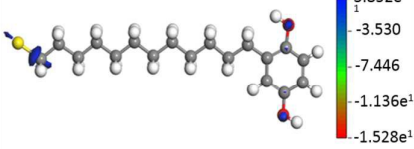
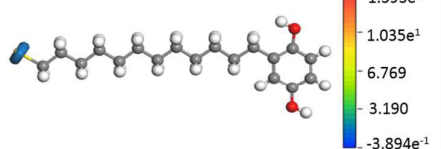
**Figure 13:** Surface Plasmon resonance when the electric field component of radiation interacts with the AuNP leading to molecular vibrations for the molecules attached to the resonating metallic surface.



**Figure 14:** (a) Unpolarised radiation interacts with the polar-stacked tail end of the indole molecule and the tail-end is stretched and compressed. (b) Unpolarised radiation interacting with the doughnut EP on the hydroquinone molecule's tail will expand and compress the tail symmetrically in all directions

Since, for polar stacked molecules, the molecules shape will dynamically change during compression- and stretching- modes, scattered photons reflect these energetics and show an enhancement in the Raman EF. However, the energetically weaker, dynamic pulsating vibration of the doughnut shaped molecule will not show the same EF enhancement.

DFT calculations were done on the 4 molecules to determine their electrophilic- and nucleophilic – centres. Figure 15 shows the resulting isosurfaces. The H-atom attached to the S-atom is not shown to better observe the nucleophilic and electrophilic centres. The S-atom and the S1 oxygen atom in coumarin act as both an electrophilic- and nucleophilic centre. For the other 3 molecules, the S-atom is only nucleophilic. For the latter 3 molecules very small electrophilic centres (area wise) are observed at the S-atom's nearest neighbour C-atom. And, in the case of indole, an electrophilic centre is observed around one of the N-atoms and one of the C-atoms in the tail region. In the case of hydroquinone similar small electrophilic centres are also observed around the tail region's O-atoms.

Ligand	Electrophilic Centre	Nucleophilic Centre
Coumarin	 S1	 S1
Indole		
Triphenylimidazole		
Hydroquinone		

**Figure 15:** Electrophilic (left) and nucleophilic (right) centres for four ligands.

The nucleophilic centre diameters were measured and is shown in figure 16. A similar trend as the EF ranking is observed with coumarin having the largest nucleophilic centre cross

sectional area, followed by indole and then triphenylimidazole and hydroquinone with more or less similar cross sectional areas. The larger Raman scattering cross-section allows for an extended interaction with electromagnetic radiation. It can therefore be concluded that the large nucleophilic centre contributes positively to the enhancement of the Raman signal.

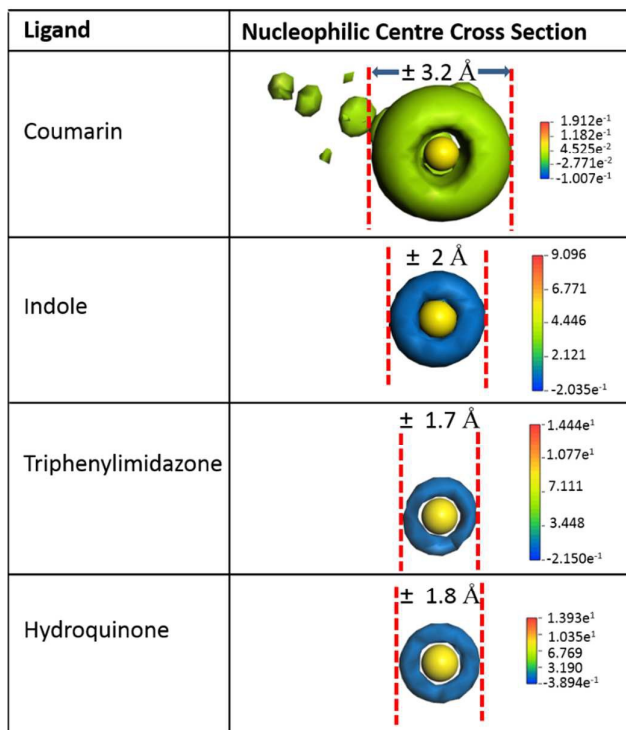


**Figure 16:** Nucleophilic centre cross section for four different ligands.

### Discussion

It was shown that the BE/ligand, molecule-surface orientation, AuNP size, positions of the HOMOs and LUMOs in both energy- and physical space, electrostatic potential and the nucleophilic centres' cross sectional areas all play a role in influencing the EF during SERS. In this qualitative assessment it can be seen that these parameters individually contribute to the experimentally observed EF trend. Thus, a functional can be postulated to express the Raman EF as follows:

$$EF \propto f(E_B, S_{NP}, \Delta, EP, \phi_N, O_{m-s}) \quad (1)$$

where  $EF$  is the enhancement factor,  $f$  some function with the following variables:  $E_b$  the BE per ligand,  $S_{NP}$  the NP diameter (size),  $\Delta$  the position of the HOMOs and LUMOs in energy

space,  $EP$  the electrostatic potential,  $\phi_N$  the nucleophilic cross sectional area and  $O_{m-s}$  is the molecule to surface orientation.

Although a constant, linear correlation between NP size and EF based on SERS has been reported<sup>40</sup> a simple analysis of the effect of NP size is not that straight forward. Since the local electromagnetic enhancement increases with the increasing particle size<sup>33</sup> it is expected that this correlation will always hold true. However, with an increase in the NP size, the convex shape of the surface also becomes much flatter. Thus the NPs will absorb less light which will lead to much less inelastic scattering that occurs on the surface and this in turn will weaken the electromagnetic field on the surface and reduce the overall SERS intensity<sup>41-44</sup>. The results from most (if not all) laboratories so far indicate that the SERS enhancement is not just highly dependent on many factors (like the size of the AuNPs) but also draws very controversial conclusions. For example, Hong *et al.*<sup>40</sup> reported that when using a different set of surfactants than this study, the optimum AuNP size that produced the maximum Raman signal enhancement was about 50 nm and that the enhancement was largely insensitive to the chemical structure of the target molecules (4-ATP and 4-NTP). On the other hand, many authors (including this study) have reported that chemical enhancement contributes greatly to the increase of Raman scattering and that the Raman enhancement is indeed sensitive to the chemical structure,<sup>26-30</sup>. It is this property that allows Raman spectroscopy to probe interfaces of multilayer structures and provide information of chemical and physical properties of a variety of organic and inorganic materials as well as the chemical composition of compound samples. When the Raman signal is enhanced, Raman can be used as a highly sensitive and selective surface analysis technique on the molecular level<sup>45-48</sup>. Thus the SERS enhancement as a function of NP size is also highly dependent on the properties of the type of molecule adsorbed to the metallic surface and the resulting chemistry associated with it. This allows for high EFs on smaller NP sizes and *vice versa*; where the SERS is directly dependent on the *type* of molecule that is under investigation and its underlying chemical and electronic properties.

## 6. Conclusion

The EFs from SERS for different AuNP-surfactant systems were measured and the observed trend was theoretically and qualitatively investigated. Four surfactants, HS-(CH<sub>2</sub>)<sub>11</sub>-NHCO-coumarin, HS-(CH<sub>2</sub>)<sub>11</sub>-NHCO-indole, HS-(CH<sub>2</sub>)<sub>11</sub>-triphenylimidazole and HS-(CH<sub>2</sub>)<sub>11</sub>-hydroquinone together with a co-stabilizing surfactant HS-(CH<sub>2</sub>)<sub>11</sub>-PEG-COOH were

adsorbed in ratios of 1% and 50% onto different sized AuNPs. Similar simulation experiments were conducted to determine the influence of the surfactant – NP BE per ligand ( $E_b$ ) on the influence of SERS. Other parameters that were qualitatively investigated were the dependency of the Raman enhancement on (a) the size of AuNPs, (b) the relative surface-to-molecule orientation, (c) the MOs (HOMOs and LUMOs), (d) the molecule electro- and nucleophilic centres and cross-sectional areas as well as (e) the molecular electrostatic potentials. It was observed that each of these parameters contribute to the final Raman signal enhancement.

### **Associated Content: Supporting Information**

The Supporting Information is available free of charge.

Materials. Instrumentation. Synthesis, functionalization and conjugation of Au nanoparticles. Calculation of the enhancement factor. Computational details. Summary of SPR bands. DFT calculated Raman Spectra. TEM images of AuNPs. Raman Spectra of AuNPs functionalized with 1% and 50% respectively of HS-(CH<sub>2</sub>)<sub>11</sub>-NHCO-coumarin, HS-(CH<sub>2</sub>)<sub>11</sub>-triphenylimidazole, HS-(CH<sub>2</sub>)<sub>11</sub>-indole and HS-(CH<sub>2</sub>)<sub>11</sub>-hydroquinone. Absorption spectra of AuNPs (14, 30 and 40 nm) functionalized with 1% and 50% respectively of HS-(CH<sub>2</sub>)<sub>11</sub>-NHCO-coumarin, HS-(CH<sub>2</sub>)<sub>11</sub>-triphenylimidazole, HS-(CH<sub>2</sub>)<sub>11</sub>-indole and HS-(CH<sub>2</sub>)<sub>11</sub>-hydroquinone. Simulated molecule-to-surface orientation for different ratios of PEG/ligand on AuNPs.

### **AUTHOR INFORMATION**

#### **Corresponding Author**

\* Email: (RAH) [harrisra@ufs.ac.za](mailto:harrisra@ufs.ac.za); [raharrisphd@gmail.com](mailto:raharrisphd@gmail.com)

#### **Notes**

The authors declare no competing financial interest.

### **ACKNOWLEDGEMENTS**

The authors would like to gratefully acknowledge the following institutions for financial support to carry out this research: University of the Free State (Physics), University of Pretoria (Physics) the Durban University of Technology (Chemistry).

### **ABBREVIATIONS**

*SERS*, surface enhanced Raman spectroscopy; *SERS EF*, surface enhanced Raman spectroscopy enhancement factors;  $E_b$ , Binding Energy; *AuNP*, Gold Nanoparticle; *NP*,

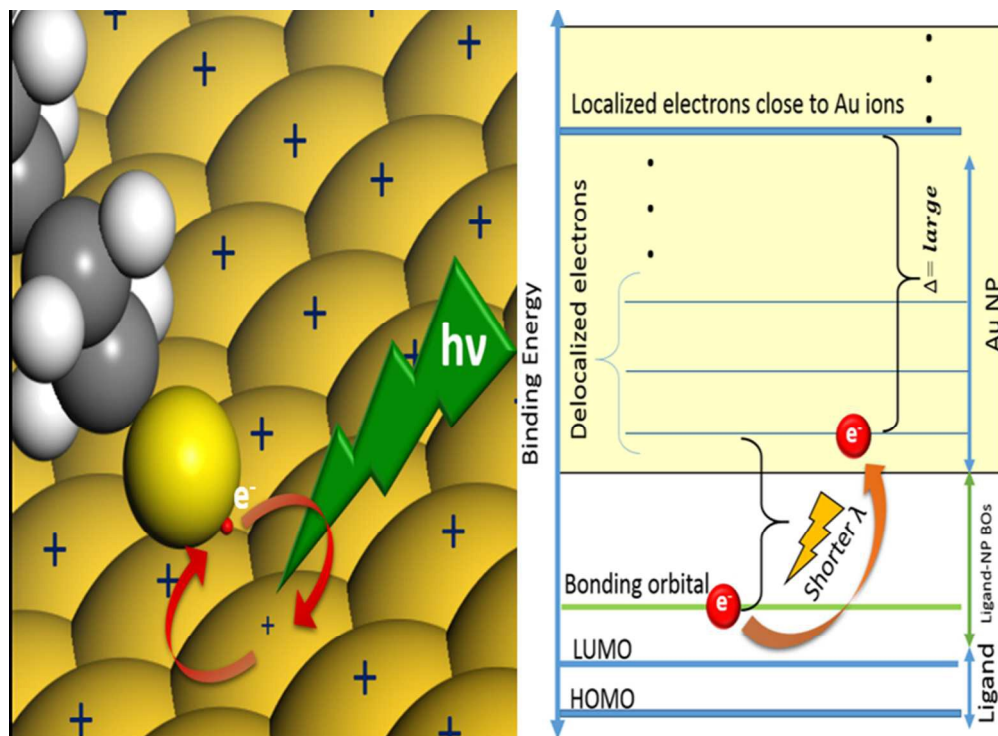
nanoparticle; *HOMO*, highest occupied molecular orbital; *LUMO*, lowest occupied molecular orbital; *SPR*, surface Plasmon resonance; *AuMMPCs*, Gold mixed monolayer protected cluster; *BO*, bonding orbital; *CB*, conduction band; *VB*, valence band; *EP*, electrostatic potential; *BE*, binding energy, *MO*, molecular orbital

## REFERENCES

- (1) G.M. Herrera, A.C. Padilla, S.P. Hernandez-Rivera, S.P. *Nanomaterials*, 2013, **3**, 158.
- (2) P. Hildebrandt, M. Stockburger, *J. Phys. Chem. B*, 1984, **88**, 5935.
- (3) X.M. Dou, Y.M. Jung, Z.Q. Cao, Y. Ozaki, *Appl. Spectrosc.*, 1999, **53**, 1440.
- (4) O.M. Primera-Pedrozo, G.D.M. Rodríguez, J. Castellanos, H. Felix-Rivera, O. Resto, S.P. Hernández-Rivera, *Spectrochim. Acta A*, 2012, **87**, 77.
- (5) Z. Hou, Z. Zhang, S. Chen, Y. Fang, N. Li, X. Zhai, Y. Liu, *Colloids Surf. A*, 2011, **384**, 345.
- (6) S. Kundu, M. Mandal, S.K. Ghosh, T. Pal, *J. Colloid Interface Sci.*, 2004, **272**, 134.
- (7) P. Photopoulos, N. Boukos, M. Panagopoulou, N. Meintanis, N. Pantiskos, Y. Raptis, D. Tsoukalas, *Procedia. Eng.*, 2011, **25**, 280.
- (8) B. Vlckova, I. Pavel, M. Sladkova, K. Siskova, M. Slouf, *J. Mol. Struct.*, 2007, **834**, 42.
- (9) O.M. Primera-Pedrozo, J.I. Jerez-Rozo, E. De La Cruz-Montoya, T. Luna-Pineda, L.C. Pacheco-Londoño, S.P. Hernandez-Rivera, *Sens. J.*, 2008, **8**, 963.
- (10) R.F. Aroca, R.A. Alvarez-Puebla, N. Pieczonka, S. Sanchez-Cortez, J.V. Garcia-Ramos, *Adv. Coll. Interf. Sci.*, 2005, **116**, 45.
- (11) K.E. Shafer-Peltier, C.L. Haynes, M.R. Glucksberg, R.P. Van Duyne, *J. Am. Chem. Soc.*, 2002, **125**, 588.
- (12) S.E.J. Bell, N.M. Sirimuthu, *Analyst*, 2004, **129**, 1032.
- (13) J.D. Driskell, O.M. Primera-Pedrozo, R.A. Dluhy, Y. Zhao, R.A. Tripp, *Appl. Spectrosc.*, 2009, **63**, 1107.
- (14) Y.W.C. Cao, R. Jin, C.A. Mirkin, *Science*, 2002, **297**, 1536.
- (15) J. Kneipp, H. Kneipp, W.L. Rice, K. Kneipp, *Anal. Chem.*, 2005, **77**, 2381.

- (16) J. Kneipp, H. Kneipp, K. Kneipp, K. *Proc. Natl. Acad. Sci.*, 2006, **103**, 17149.
- (17) H. Wackerbarth, U. Klar, W. Gunther, P. Hildebrandt, *Appl. Spectrosc.*, 1999, **53**, 283.
- (18) T. Vo-Dinh, F. Yan, M.B. Wabuyele, *J. Raman Spectrosc.*, 2005, **36**, 640.
- (19) I. López-Tocón, S.P. Centeno, J.C. Otero, J.I. Marcos, *J. Mol. Struct.*, 2001, **565**, 369.
- (20) Z. Luo, Y. Fang, *J. Colloid Interface Sci.*, 2006, **301**, 184.
- (21) L. Xia, J. Wang, S. Tong, G. Liu, J. Li, H. Zhang, *Vibrational Spectroscopy*, 2008, **47**, 124.
- (22) Y. Wang, H. Wei, B. Li, W. Ren, S. Guo, S. Dong, E. Wang, *Chemical Communications*, 2007, **48**, 5220.
- (23) S. Nie, S.R. Emory, *Science*, 1997, **275**, 1102.
- (24) R.J. Dijkstra, W.J.J.M. Scheenen, N. Dam, E.W. Roubos, J.J. Ter Meulen, *J. Neurosci. Meth.*, 2007, **159**, 43.
- (25) J. Ni, R.J. Lipert, G.B. Dawson, M.D. Porter, *Analytical Chemistry*, 1999, **71**, 4903.
- (26) M. Moskovits, *Nature*, 2010, **464**, 357.
- (27) R.A. Alvarez-Puebla, L.M. Liz-Marz'an, *Small*, 2010, **6**, 604.
- (28) I. Mannelli, M.P. Marco, *Analytical and Bioanalytical Chemistry*, 2010, **398**, 2451.
- (29) T. Vo-Dinh, H.N. Wang, J. Scaffidi, *Journal of Biophotonics*, 2010, **3**, 89.
- (30) J. Kneipp, H. Kneipp, B. Wittig, K. Kneipp, *Nanomedicine*, 2010, **6**, 214.
- (31) A.D. McFarland, M.A. Young, J.A. Dieringer, R.P. Van Duyne, *J. Phys. Chem. B*, 2005, **109**, 11279.
- (32) S.R. Emory, W.E. Haskins, S. Nie, *J. Am. Chem. Soc.*, 1998, **120**, 8009.
- (33) K.L. Kelly, E. Coronado, L.L. Zhao, G.C. Schatz, *J. Phys. Chem. B*, 2003, **107**, 668.
- (34) W.C. Lin, S.H. Huang, C.L. Chen, C.C. Chen, D.P. Tsai, H.P. Chiang, *Appl. Phys. A*, 2010, **101**, 185.
- (35) R.A. Harris, P.M. Shumbula, H. Van der Walt, *Langmuir*, 2015, **31**, 3934.

- (36) S.M. Morton, L. Jensen, *J. Am. Chem. Soc.*, 2009, **131**, 4090.
- (37) M. Kerker, D.S. Wang, H. Chew, *Appl. Opt.*, 1980, **19**, 3373.
- (38) D. Becerril, C. Noguez. *J. Phys. Chem. C*, 2015, **119**, 10824.
- (39) A. Barnard, *Cryst. Growth Des.*, 2013, **13**, 5433.
- (40) S. Hong, X. Li, *Journal of Nanomaterials*, 2013, **2013**, 1.
- (41) S.C. Boca, C. Farcau, S. Astilean, *Nuclear Instruments and Methods in Physics Research Section B*, 2009, **267**, 406.
- (42) S. Ghoshal, D. Mitra, S. Roy, D.D. Majumder, *Sensors and Transducers Journal*, 2010, **113**, 1.
- (43) S.A. Maie, *Plasmonics: Fundamentals and Applications*, Springer, New York, NY, USA, 1st edition, 2007.
- (44) M. Moskovits, *Reviews of Modern Physics*, 1985, **57**, 783.
- (45) S. Kundu, *Journal of Materials Chemistry C*, 2013, **1**, 831.
- (46) S. Kundu, M. Jayachandran, *RSC Advances*, 2013, **3**, 16486.
- (47) D. Majumdar, A. Singha, P. K. Mondal, S. Kundu, *ACS Appl. Mater. Interfaces*, 2013, **5**, 7798.
- (48) U. Nithiyantham, S.R. Ede, S. Kundu, *J. Mater. Chem. C*, 2014, **2**, 3782.



141x102mm (150 x 150 DPI)